AGU PUBLICATIONS

Space Weather

RESEARCH ARTICLE
10.1002/2014SW001083

Key Points:
- Developed tool to compute magnetic perturbations on the ground
- Too validated using existing SWMF implementation
- Model validation independent from Delta-B calculation within each model

Supporting Information:
- Readme
- Figure S1
- Figure S2
- Figure S3
- Figure S4
- Figure S5
- Figure S6
- Figure S7
- Figure S8
- Figure S9
- Figure S10
- Figure S11
- Figure S12

Correspondence to:
L. Rastätter,
Lutz.Rastaetter@nasa.gov

Citation:
Rastätter, L., G. Tóth, M. M. Kuznetsova, and A. A. Pulkkinen (2014), CalcDeltaB: An efficient postprocessing tool to calculate ground-level magnetic perturbations from global magnetosphere simulations, *Space Weather*, *12*, 553–565, doi:10.1002/2014SW001083.

Received 28 MAY 2014
Accepted 9 SEP 2014
Accepted article online 13 SEP 2014
Published online 1 OCT 2014

CalcDeltaB: An efficient postprocessing tool to calculate ground-level magnetic perturbations from global magnetosphere simulations

Lutz Rastätter[1], Gábor Tóth[2], Maria M. Kuznetsova[1], and Antti A. Pulkkinen[1]

[1]Community Coordinated Modeling Center, Space Weather Laboratory, NASA Goddard Space Flight Center, Greenbelt, Maryland, USA, [2]Center for Space Environment Modeling, University of Michigan, Ann Arbor, Michigan, USA

Abstract Ground magnetic field variations can induce electric currents on long conductor systems such as high-voltage power transmission systems. The extra electric currents can interfere with normal operation of these conductor systems; and thus, there is a great need for better specification and prediction of the field perturbations. In this publication we present CalcDeltaB, an efficient postprocessing tool to calculate magnetic perturbations $\Delta\mathbf{B}$ at any position on the ground from snapshots of the current systems that are being produced by first-principle models of the global magnetosphere-ionosphere system. This tool was developed during the recent "d*B*/d*t*" modeling challenge at the Community Coordinated Modeling Center that compared magnetic perturbations and their derivative with observational results. The calculation tool is separate from each of the magnetosphere models and ensures that the $\Delta\mathbf{B}$ computation method is uniformly applied, and that validation studies using $\Delta\mathbf{B}$ compare the performance of the models rather than the combination of each model and a built-in $\Delta\mathbf{B}$ computation tool that may exist. Using the tool, magnetic perturbations on the ground are calculated from currents in the magnetosphere, from field-aligned currents between magnetosphere and ionosphere, and the Hall and Pedersen currents in the ionosphere. The results of the new postprocessing tool are compared with $\Delta\mathbf{B}$ calculations within the Space Weather Modeling Framework model and are in excellent agreement. We find that a radial resolution of $1/30\ R_E$ is fine enough to represent the contribution to $\Delta\mathbf{B}$ from the region of field-aligned currents.

1. Introduction

At the Community Coordinated Modeling Center (CCMC), numerical models of the plasma and fields of the solar corona, heliosphere, global magnetosphere, inner magnetosphere, and the ionosphere/thermosphere of the Earth are hosted, and simulation runs are made available to researchers through the center's run-on-request system. Model outputs can be viewed and analyzed via online visualization and postprocessing tools and enable scientists to do their research without having to run the models themselves. Besides the run-on-request system, classes of models (e.g., global magnetosphere or ionosphere/thermosphere models) are tested against observational data in modeling challenges.

One of these challenges is the community-wide Geospace research-to-operation "d*B*/d*t*" challenge [*Pulkkinen et al.*, 2013] that was initiated in 2010 by a request from the Space Weather Prediction Center (SWPC) of the National Oceanic and Atmospheric Administration (NOAA). The interest in d*B*/d*t* is driven by the increased awareness about space weather impacts on high-voltage power transmission systems. The variations in the geomagnetic field, d*B*/d*t*, induce geomagnetically induced currents (GIC) that can be problematic for normal operation of the power transmission systems. The heightened awareness about the GIC issues is illustrated also by the ongoing action by the U.S. Federal Energy Regulatory Commission to develop standards for mitigating the hazard. Consequently, there is a great interest in characterizing and predicting d*B*/d*t*. The d*B*/d*t* study required the development of a stand-alone postprocessing tool to calculate magnetic perturbations on the ground at any position from electric currents that are output by global magnetosphere-ionosphere simulation models. The stand-alone tool is extremely valuable for the following two reasons:

1. Three first-principle models of the global magnetosphere, coupled to ionospheric electrodynamics models, entered the challenge. Only one of the models, the Space Weather Modeling Framework (SWMF), possesses the capability to compute magnetic perturbations on the ground from all current systems in

Table 1. Event Numbers With Dates, Minimum *Dst*, and Maximum *Kp*[a]

Event #	Date and UT Time	min(*Dst*) (nT)	Max(*Kp*)
1	29 Oct 2003 06:00 to 30 Oct 2003 06:00	−353	9
2	14 Dec 2006 11:30 to 6 Dec 2006 00:00	−139	8
3	31 Aug 2001 00:00 to 1 Sep 2001 00:00	−40	4
4	31 Aug 2005 09:30 to 1 Sep 2005 12:00	−131	7
5	5 Apr 2010 00:00 to 6 Apr 2010 00:00	−50*	8−
6	5 Aug 2011 09:00 to 6 Aug 2011 09:00	−107*	8−

[a] *Dst* values marked with (*) are provisional.

the coupled system. By developing the stand-alone tool, the other models' outputs can be processed and compared to magnetometer data as well. Magnetosphere-ionosphere models that have not been included in the d*B*/d*t* study can be supported by the tool in the future. This will include the Grand Unified Magnetosphere-Ionosphere Coupled Simulation (GUMICS) model, currently available in the serial (one processor) version 4 at the CCMC.

2. The stand-alone tool can be run with the same parameters (e.g., the radial resolution in a grid needed to calculate the contribution from field-aligned currents) for all the models rather than depending on algorithms and parameters that may differ between the models. Thus, a validation can assess the performance of each model separate from the performance of the Δ**B**-calculation method.

The study, referred to as the d*B*/d*t* study in the remainder of this paper, has been conducted by the Community Coordinated Modeling Center (CCMC) to assess the ability of space weather forecast models to predict magnetic perturbations on the ground at selected magnetometer sites that, in turn, can be used to estimate the probability of large GIC during geomagnetically active times. The d*B*/d*t* study is based on six storm and substorm events that contain a large range of geomagnetic states. The study and the events are described in detail in *Pulkkinen et al.* [2013]. The event dates and geomagnetic activity indices are also listed in Table 1. The primary goals of the d*B*/d*t* challenge were to evaluate strengths and weaknesses and differences between the available modeling approaches.

This paper reports on the CalcDeltaB tool that is used to postprocess magnetosphere model outputs at the CCMC to compute magnetic perturbations on the ground from the three global magnetosphere models that were included in the study. We have developed the tool in three separate components that calculate magnetic perturbations from ionospheric currents, field-aligned currents, and magnetospheric currents. We describe in detail the implementation of our computation and find the optimal grid resolution parameter used in the gap region between ionosphere and magnetosphere and compare the outputs of each component with the outputs from similar calculations [*Yu et al.*, 2010] that are implemented in the Space Weather Modeling Framework [*Tóth et al.*, 2005, 2012]. We verify the correctness of our calculations with analytically tractable problems and explain differences between the results from the SWMF model implementation and our postprocessing tool.

CalcDeltaB does not include effects caused by the presence of Earth which include shielding and inducted fields due to the conductivity distribution below ground level. To accurately account for the induction effects, the knowledge of the time history of all electric currents is required together with detailed ground conductivity structure. Carrying out such detailed electrodynamic treatment of these effects was beyond the scope provided by the d*B*/d*t* challenge that also governs this paper.

Using the newly developed tool, we report relative strength of contributions from the different current systems as obtained by our calculations during the six events. In *Pulkkinen et al.* [2013] and in the report to SWPC, the time derivative of the horizontal (northward and eastward) magnetic perturbations (ΔB_N, ΔB_E) are used. The Δ**B** and d*B*/d*t* values (approximate time derivatives computed from 1 min time series) are basis for the time series plots and skill scores that are available through an online plotting and analysis tool on the CCMC website.

2. Setup of the Challenge

During the definition of the d*B*/d*t* challenge, described in detail in *Pulkkinen et al.* [2013], CCMC and SWPC staff members and the modelers that were involved in the challenge decided to use 1 min averages of the time derivative of the horizontal magnetic perturbation, which is composed of northward (ΔB_N) and

Table 2. Magnetometer Stations Used in the 2008 GEM Modeling Challenge[a]

Station		Geographic		Geomagnetic	
Name	IAGA Code	Latitude	Longitude	Latitude	Longitude
Fresno	FRN	37.09	240.28	43.52	305.25
Newport	NEW	48.27	242.88	54.85	304.68
Meanook	*MEA*	54.62	246.65	61.57	306.20
Yellowknife	*YKC*	62.48	245.52	68.93	299.36
Fredericksburg	FRD	38.20	282.63	48.4	353.38
Ottawa	*OTT*	45.40	284.45	55.63	355.31
Poste de la Baleine	*PBQ*	55.28	282.26	65.46	351.81
Iqaluit	IQA	63.75	291.48	73.98	5.24
Fürstenfeldbrück	FUR	48.17	11.28	48.38	94.61
Wingst	*WNG*	53.74	9.07	54.12	95.00
Abisko	*ABK*	68.36	18.82	66.06	114.66
Hornsund	HRN	77.00	15.37	73.88	125.99

[a]The ones selected for the d*B*/d*t* study are shown in italics. The table lists the stations by chain from low- to high-magnetic latitudes (for year 2000).

eastward (ΔB_E) components of the magnetic perturbation at each magnetometer location. Magnetic perturbations in the study were determined at each magnetometer station by taking the average of quiet days near the event dates and subtracting this average diurnal variation ("baseline") from the observations during the event days. Six Geospace events were selected that represent a range of different geomagnetic activity levels. All events with their start and end dates and times, minimum *Dst*, and maximum *Kp* index values are listed in Table 1. The computation of magnetic perturbations developed for the d*B*/d*t* study expands the work of *Yu et al.* [2010] by calculating $\Delta\mathbf{B}$ for new events and different magnetometer stations. In addition, we establish a set of numerical parameters that enables us to perform the calculation as a postprocessing step and derive $\Delta\mathbf{B}$ values from currents that were calculated by three of the four coupled magnetosphere-ionosphere models that are available for "Runs-on-Request" at the CCMC.

3. Magnetometer Stations Used

Twelve magnetometer stations (four each from three chains in Europe, eastern, and western North America) were selected for the 2008 GEM challenge [*Pulkkinen et al.*, 2011] (Table 2). Of those, only the stations in high latitudes or auroral latitudes and midlatitudes have been used in the research-to-operation study [*Pulkkinen et al.*, 2013]. The names are indicated in italics in Table 2. In our tool we use the geographic positions of the stations and use the GEOPACK 2008 library (http://geo.phys.spbu.ru/~tsyganenko/modeling.html) to determine the magnetic dipole coordinate (MAG) positions for each station for each event. This takes into account the slowly time-dependent nature of MAG positions as opposed to the SWMF implementation that uses the MAG positions for the 2000 epoch year (listed in Table 2) and a fixed orientation of the Earth's dipole field.

4. Simulation Model

The Space Weather Modeling Framework (SWMF) [*Tóth et al.*, 2005, 2012] is the only model that directly calculates the magnetic perturbation on the ground derived from all the currents in the modeled magnetosphere-ionosphere system [*Yu et al.*, 2010]. For the d*B*/d*t* study, SWMF was run as a combination of the magnetosphere MHD component Block-Adaptive-Tree-Solarwind-Roe-Upwind-Scheme [*Powell et al.*, 1999] coupled to the Rice Convection Model [*Wolf et al.*, 1991] and the Ridley Ionosphere Model [*Ridley et al.*, 2004]. The development of the postprocessing tool to compute $\Delta\mathbf{B}$ values on the ground is a vital step in the d*B*/d*t* challenge since other magnetosphere models included in the challenge (OpenGGCM [*Raeder et al.*, 2001] and Lyon-Fedder-Mobarry (LFM) [*Lyon et al.*, 2004; *Wiltberger et al.*, 2004; *Merkin and Lyon*, 2010]) do not calculate $\Delta\mathbf{B}$ values.

To cross validate the results of our calculation of ground magnetic perturbations, results from SWMF have been used in this paper. For the purposes of this paper we use both the model's own output of $\Delta\mathbf{B}$ (ID: 9a_SWMF) and the results from the postprocessing of global magnetospheric and ionospheric current systems to compute $\Delta\mathbf{B}$ (ID: 9_SWMF). The SWMF model and the postprocessing calculation were run for all six events and are now routinely run in this or similar configurations for Runs-on-Request at the CCMC.

Outputs of the magnetosphere and the ionosphere electrodynamics of the SWMF model provide the current densities used in the calculation of the magnetic perturbations which are described in the next section.

5. Implementation of CalcDeltaB

In the CalcDeltaB tool, the $\Delta\mathbf{B}$ values are calculated from three contributions in the magnetosphere-ionosphere system: from the current densities in the magnetosphere, the height-integrated current densities in the ionosphere, and the field-aligned currents that connect the ionosphere solution to the magnetosphere. The ionosphere currents are calculated by an ionospheric electric potential solver that is used to define the ionospheric boundary conditions for the magnetosphere model. Magnetosphere and ionosphere are linked by the field-aligned currents that are assumed to flow along dipole field lines between the inner boundary of the magnetosphere and the ionospheric altitude. The calculations to obtain $\Delta\mathbf{B}$ from each of the current systems are explained in detail in the following sections.

5.1. Magnetosphere Currents

Electric currents from the magnetosphere model are used to calculate the magnetic perturbation $\Delta\mathbf{B}$ by using the Biot-Savart formula:

$$\Delta\mathbf{B} = \frac{\mu_0}{4\pi} \sum_{|X_J|>R_0} \frac{\mathbf{J}\times\mathbf{R}}{\mathbf{R}^3} dV. \tag{1}$$

Here $\mathbf{R} = \mathbf{X}_J - \mathbf{X}_{\text{station}}$ is the vector between the position of the current element $\mathbf{X}_J$ at each grid cell center and the magnetometer position ($\mathbf{X}_{\text{station}}$), and dV is the volume of the grid cell that has current density $\mathbf{J}$. To be included in the summation cell center positions, $\mathbf{R}$ must be at least R_0 from the Earth's center: Every MHD model of the magnetosphere has a near-Earth boundary that is separated from the ionosphere electrodynamics boundary by a certain distance to avoid the very strong magnetic field and large Alfvén velocities that restrict the maximum allowed time step in the numerical schemes [*Powell et al.*, 1999; *Raeder et al.*, 2001; *Lyon et al.*, 2004; *Wiltberger et al.*, 2004]. The near-Earth boundary for the SWMF is typically located at $R_B = 2.5\ R_E$ from the Earth's center. To ensure numerical accuracy, currents that are mapped into the ionosphere are taken from inside the magnetosphere grid at $R_0 = 3\ R_E$, similar to the distance of $R_0 = R_B + 1\ R_E = 3.5\ R_E$ cited by *DeZeeuw et al.* [2004] and *Ridley et al.* [2004]. The margin $R_0 - R_B = 0.5\ R_E$ is larger than a near-Earth cell size $\Delta x = 0.25\ R_E$.

5.2. Ionospheric Currents

We use the original model grid in the ionosphere and the Cartesian components of the ionospheric height-integrated current density (J_x, J_y, J_z) reported by the ionosphere electrodynamic models. The size of the surface elements dS at each ionosphere grid position is given by

$$dS = r_{\text{iono}}^2 \cos\lambda\, d\phi\, d\lambda, \tag{2}$$

with $d\phi$ and $d\lambda$ the distance between adjacent grid positions in the azimuthal and latitudinal direction, respectively. We use the Biot-Savart formula (equation (1)) for the ionosphere currents in the same manner as for the magnetosphere substituting dS for the magnetospheric grid cell volume dV and the height-integrated ionospheric current density J (measured in A/m) for the magnetosphere current density (measured in units of A/m^2).

5.3. Field-Aligned Currents

The field-aligned currents (FACs) fill the gap region between the R_0 (section 5.1) and the ionosphere (at 110 km altitude). During postprocessing the magnetic field-aligned currents (FACs) are picked up from the magnetosphere and assumed to follow a dipole magnetic field to the ionosphere. We use the grid and the radial current density (J_r) at 110 km altitude reported by the ionosphere electrodynamics model. The region between 110 km ($r_{\text{iono}} = (1. + 110/6371.2)\ R_E = 1.01727\ R_E$) and the pickup radius of the magnetospheric currents at R_0 is represented by a spherical grid with an adjustable radial grid spacing and the model's grid in the ionosphere for longitude (azimuth) angles ϕ between 0 and 2π and latitude angles λ between $-\pi/2$ at the South Pole and $\pi/2$ at the North Pole. FACs are arranged on filaments emanating from the ionosphere grid that run along lines of the dipolar magnetic field $\mathbf{B}_{\text{dip}}$ which determines the orientation and strength

of the FACs in the gap region. In spherical coordinates (r, ϕ, λ) the dipole field with Earth's magnetic dipole moment **m** is

$$\mathbf{B}_{\text{dip}} = \frac{3(\mathbf{m}\cdot\mathbf{r})\mathbf{r} - r^2\mathbf{m}}{r^5} = \frac{B_{\text{eq}}}{r^3}\begin{pmatrix} 2\sin\lambda \\ 0 \\ -\cos\lambda \end{pmatrix}. \tag{3}$$

Radius r is in units of $R_E = 6371.2$ km, and $B_{\text{eq}} = 31100$ nT is the field strength at the Earth's surface. From equation (3) the magnetic field strength is

$$B_{\text{dip}}(r, \lambda) = B_{\text{eq}}\frac{\sqrt{3\sin^2\lambda + 1}}{r^3}. \tag{4}$$

One can also derive from equation (3) that along any dipole field line the following equation holds

$$r\cos^2\lambda = r_{\text{iono}}\cos^2\lambda_{\text{iono}}. \tag{5}$$

Equation (5) is used to calculate the latitude $\lambda(r, \lambda_{\text{iono}})$ along a dipole field line on each radial level of the grid (r) for each footprint located at λ_{iono} and r_{iono} in the ionosphere. Each volume element in the FAC region is then computed for each filament (index i) using the half distance between adjacent filaments (located at index $[j-1]$ and $[j+1]$):

$$dV_{i,j} = dr\,(r_i)^2\frac{\lambda_{j+1} - \lambda_{j-1}}{2}\cos\lambda_j. \tag{6}$$

For the polar axes ($j = 1$: south, $j = N$: north), the expression of equation (6) is replaced by

$$dV_{i,1} = dr\,(r_i)^2\frac{\lambda_2 - \left(-\frac{\pi}{2}\right)}{2}\cos\left(\frac{\lambda_1 + \left(-\frac{\pi}{2}\right)}{2}\right) \tag{7}$$

$$dV_{i,N} = dr\,(r_i)^2\frac{\frac{\pi}{2} - \lambda_{N-1}}{2}\cos\left(\frac{\lambda_{N-1} + \frac{\pi}{2}}{2}\right). \tag{8}$$

The finite difference in latitude angle in equation (6), which involves positions across the pole, is replaced by the latitude difference between the respective pole and the first element of λ adjacent to the pole. The argument of the cosine in equation (6) is being replaced by the half distance between the polar axis and the first grid position away from the polar axis as shown in equations (7) and (8). This is needed to obtain the volume elements that fill the region around the axes.

To obtain the current strength in each FAC filament, we use the radial component of the FACs (J_r) that is reported by the output provided by the ionosphere electrodynamics module of SWMF (and other magnetosphere-ionosphere coupled models). J_r results from current densities that are encountered at the current pickup radius R_0 in the magnetosphere and mapped into the ionosphere. To obtain the strength and sign of the actual field-aligned currents, J_r is divided by the sine of the dipole inclination angle I (derived from the r and λ components of the dipole field in equation (3)).

$$I = \arctan\left(\frac{2\sin\lambda_{\text{iono}}}{\cos\lambda_{\text{iono}}}\right). \tag{9}$$

The ratio of the field strength (Equation (4)) at the grid position on the FAC filament divided by the magnetic field strength at the ionosphere foot point is used to scale the current at the ionosphere altitude to yield the current strength along the filament:

$$\mathbf{J}_{\text{FAC}}(r, \phi, \lambda) = \frac{J_r(\phi, \lambda_{\text{iono}})}{-\sin I}\frac{1}{r^3}\begin{pmatrix} 2\sin\lambda \\ 0 \\ -\cos\lambda \end{pmatrix}\frac{r_{\text{iono}}^3}{\sqrt{3\sin^2\lambda_{\text{iono}} + 1}}. \tag{10}$$

As with magnetosphere currents, magnetic perturbations from FACs are calculated using the Biot-Savart formula (equation (1)). In contrast to the *Dst* study [*Rastätter et al.*, 2013], the contribution of the field-aligned currents to the magnetic perturbations at the magnetometer stations is nonnegligible. The distance vector

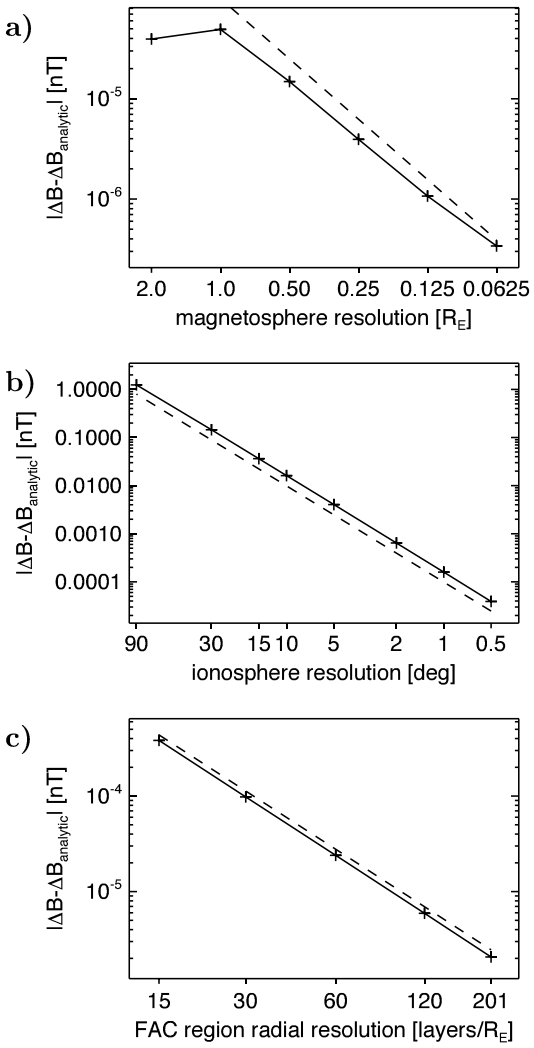

Figure 1. Grid convergence for magnetosphere, FACs, and ionosphere contributions to $\Delta\mathbf{B}$. Differences between the analytical and numerical representations of $|\Delta\mathbf{B}|$ are shown: (a) Shows how well the magnetic perturbation from a line current in the magnetosphere represented by finite-size grid cells compares to the analytical prediction for the Earth's center. (b) Shows how the signal from a current loop in the ionosphere is resolved at different angular spacings along the loop. (c) Shows how well the $\Delta\mathbf{B}_{East}$ at station YKC from a FACs along the northern polar axis is represented using different radial resolutions. In each plot the finest resolutions are shown on the right. The slope of the dashed line in each panel indicates second-order convergence.

(**R**) between the FAC element and the station position is not always in the poloidal plane unlike the vector from the Earth's center to the current element in the case of the *Dst* calculation. The sum of all FAC elements may have nonzero components in each of the three directions. In addition, we have to consider local magnetic north, east, and downward components of $\Delta\mathbf{B}$ at each station location instead of a single component aligned with the magnetic dipole axis for *Dst*.

5.4. Local Magnetic Coordinate System

After combining the three contributions in solar magnetospheric (SM) coordinates, the three cartesian components of $\Delta\mathbf{B}$ are converted to (North, East, and Down) or (λ, ϕ, and $-r$) components in local spherical coordinates at each station. In the dB/dt study, the horizontal components (North and East) are used to compute the time derivatives that are then compared to the respective components reported by each station.

6. Verification of Calculation Method

In this section we show that the implemented algorithms of CalcDeltaB work correctly and accurately. We calculate the magnetic perturbations due to the three current systems for cases where an analytic solution is known and check that the numerical solution converges to the analytic solution with the expected rate of convergence. We also perform a cross validation of our code with the SWMF implementation for some of the simulated events. Based on the results, we establish the minimum grid resolution needed in the FAC region for efficient calculations with an acceptable accuracy.

The simulation results obtained with the calculation of ΔB inside the SWMF are given the identifier "9a_SWMF" in the publication of the study [*Pulkkinen et al.*, 2013], the report issued by the CCMC for NOAA SWPC and online visualization of the results at the CCMC website. The temporal resolution of 1 min was required in the dB/dt study. To achieve real-time speed in operational mode, it must take less than a minute for the postprocessing calculation to generate the $\Delta\mathbf{B}$ values at all the station locations from snapshots of all the current systems that are output by the model after each 1 min simulation time interval.

6.1. Test of Magnetosphere Contribution

The validity of our approach to the Biot-Savart integration was tested with a line current in the magnetosphere that extends along a constant position in X and Z across the simulation domain from $-128\ R_E$ to $+128\ R_E$ in Y. Figure 1a shows the difference between the numerical and analytical value of $|\Delta\mathbf{B}|$ resulting from a magnetosphere line current that flows through the magnetosphere box in the Y direction. The current we used for testing is located in a square of $(\Delta x)^2$ cross section centered at $X_M = 30\ R_E$ and $Z_M = 0\ R_E$ using $R_E = 6371.0008$ km. The current flows along the Y direction through the entire magnetosphere grid

($|Y| \le Y_0$, $Y_0 = 128\ R_E$). Its strength is $I = 1\ \mu A/m^2\ R_E^2 = 40.58965$ MA. The expected field strength at position (X, Y, Z) is given by

$$|B_{\text{analytic}}| = \frac{\mu_0 I}{4\pi R} \frac{2Y_0}{\sqrt{Y_0^2 + R^2}}$$
$$R^2 = (X_M - X)^2 + (Z_M - Z)^2. \tag{11}$$

For the Earth's center ($X = 0, Y = 0, Z = 0$), we have $R = 30\ R_E$ and the expression in equation (11) yields $|B_{\text{analytic}}| = 41.35273$nT. In Figure 1a, between the resolution of 1 R_E and 1/8 R_E, we see second-order grid convergence toward the analytic value, indicated by the slope of the dashed line (proportional to the square of the grid spacing) that runs parallel to our results (solid line).

6.2. Test of Ionosphere Current Contribution

The ionosphere current integration was tested with a ring of current located at the equator with a strength of 111 kA (equivalent to a current density of 1 μA/m in a band of 1° width around the equator). The analytic expression of a magnetic field generated in the vicinity of a closed current loop can be expressed in cylindrical coordinates (ρ, ϕ, z) with complete elliptic integrals for the first and second kind K and E, respectively (*Griffiths* [1950], page 271):

$$B_\rho = \frac{\mu_0 I}{2\pi} \frac{z}{[(a+\rho)^2 + z^2]^{\frac{1}{2}}} \left[-K(m) + \frac{a^2 + \rho^2 + z^2}{(a-\rho)^2 + z^2} E(m)\right]$$
$$B_\phi = 0$$
$$B_z = \frac{\mu_0 I}{2\pi} \frac{1}{[(a+\rho)^2 + z^2]^{1/2}} \left[K(m) + \frac{a^2 - \rho^2 - z^2}{(a-\rho)^2 + z^2} E(m)\right], \tag{12}$$

with parameter $m = 4a\rho/[(a+\rho)^2 + z^2]$ and $a = R_E + 110$ km being the radius of the current ring. To calculate numerical values we used the approximation formula 17.3.34 for $K(m)$ and 17.3.36 for $E(m)$ in *Abramowitz* [2010] to calculate the function values to within $2 \cdot 10^{-8}$. At station YKC the analytic expression yields $\Delta B_{\text{Down}} = -4.226360$ nT, $\Delta B_{\text{East}} = 0$, $\Delta B_{\text{North}} = 0.402480$ nT, and strength $|B_{\text{analytic}}| = 4.245481$. Figure 1b shows that the numerical result for $|\Delta B|$ approaches the analytical value with a second-order convergence rate, reaching 0.01% accuracy at 1° resolution.

6.3. Test of Contribution From Field-Aligned Current Region

The region that holds the field-aligned currents (FACs) between the magnetosphere's inner boundary and the altitude of the ionosphere boundary is filled with a spherical grid. The grid starts with the latitude and longitude positions as defined in the ionosphere electrodynamics module of the coupled ionosphere-magnetosphere model. In the case of SWMF, the ionosphere grid has 1° spacing in latitude and a 2° spacing in longitude. The radial resolution is a free parameter of the postprocessing algorithm as well as in the SWMF model itself. The SWMF model version used for the study utilized 800 layers.

We performed a test of the FAC integration by specifying a current along the North Pole axis. The FAC integration should result in an east component of strength

$$\Delta B_{\text{FAC,East}} = \frac{\mu_0 I}{4\pi r_0} \left[\frac{z_2 - z_0}{\sqrt{(z_2 - z_0)^2 + r_0^2}} - \frac{z_1 - z_0}{\sqrt{(z_1 - z_0)^2 + r_0^2}}\right], \tag{13}$$

with $z_1 = R_E + 110$ km $= 1.01727\ R_E$, $z_2 = 3\ R_E$, $r_0 = \cos\lambda\ R_E$, and $z_0 = \sin\lambda\ R_E$. For YKC ($\lambda = 68.93\pi/180$) and current of $I = 1\ \mu A/m^2 \pi R_1^2 (0.5\pi/180)^2 = 10$ kA, the field should equal 0.3323795 nT. Figure 1c shows the difference between the analytical and numerical results depending on the radial grid resolution (represented by the number of layers per R_E). As with the magnetosphere contribution, second-order convergence is achieved.

During our separate postprocessing, we only rely on a few processors to perform the calculation for each time step; and therefore, we must limit the size of the radial grid if we want to perform the calculation efficiently. To be suitable for real-time operations in combination with any magnetosphere model other than SWMF (such as LFM or OpenGGCM), the postprocessing tool needs to complete a calculation before the

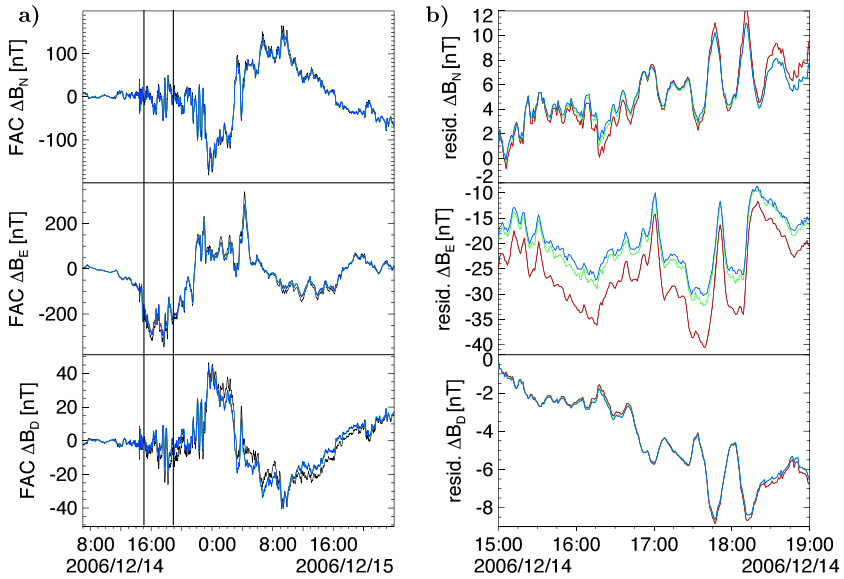

Figure 2. Field-aligned current contribution to **ΔB** for station YKC and differences between CalcDeltaB and SWMF. (a) The contribution from FACs calculated by SWMF (black) and by CalcDeltaB (colors). (b) The residuals between CalcDeltaB and SWMF from 15:00 UT to 19:00 UT on 14 December (interval between the vertical lines in Figure 2a for different radial resolutions: red, $dr = 1/15\ R_E$; green, $dr = 1/30\ R_E$; light blue, $dr = 1/60\ R_E$; and dark blue, $dr = 1/120\ R_E$. In the global view of Figure 2a, all CalcDeltaB traces are mostly identical and the dark blue ($dr = 1/120\ R_E$) is seen only. In the residuals in Figure 2b, the traces for $dr = 1/15\ R_E$ (red, lowest trace in the East component, middle panel) and for $dr = 1/30\ R_E$ (green, middle trace in the East component) are distinguishable from the traces for $dr = 1/60\ R_E$ and $dr = 1/120\ R_E$ (light blue and dark blue, respectively) that are on top of each other.

magnetosphere model outputs another snapshot of the current system. Thus, the FAC calculation needs to complete in less than a minute during real-time operations given the 1 min output cadence required by SWPC and used in the d*B*/d*t* study. To determine what resolution is required to get a reasonably accurate solution, we performed a grid convergence test using radial spacings of $1/15\ R_E$, $1/30\ R_E$, $1/60\ R_E$, $1/120\ R_E$, and $1/201\ R_E$ corresponding to 29, 59, 118, 237, and 400 layers between $1.017\ R_E$ (110 km altitude) and $3\ R_E$, respectively. Results are shown in Figure 2 for two stations for the "AGU Storm" (Event 2). Figure 2a shows CalcDeltaB and SWMF model results for the **ΔB** signal from FACs at Yellowknife (YKC). The colored traces are from the different radial resolutions (red: $1/15\ R_E$, green: $1/30\ R_E$, light blue: $1/60\ R_E$, and dark blue: $1/120\ R_E$). The results for the four resolutions are very similar and for most times lie on top of each other (masked by the dark blue line). Figure 2b shows the differences between CalcDeltaB and SWMF results for the four radial resolutions mentioned above. We see that resolutions of 1/30 and finer yield nearly identical results and only $1/15\ R_E$ differs noticeably more from the SWMF results than the other resolutions. In addition to the visual result that indicates that a radial resolution of $1/30\ R_E$ will yield results that are as close as possible to the SWMF results, skill score calculations do not show any differences at higher resolutions. Finer resolutions than $1/30\ R_E$ yield no better results and consume unnecessary computing cycles. Computational effort in terms of central processing unit (CPU) usage grows proportional to the number of layers per R_E and reaching a full minute of CPU time for the 12 stations in the challenge for the finest resolution. We chose $dr = 1/30\ R_E$ for the model challenge described in *Pulkkinen et al.* [2013]. This resolution allows for real-time calculation of the contribution while providing good results with minimal use of computing resources.

6.3.1. Elimination of FAC Filaments Below a Significance Threshold

A possible way to save computational time is to eliminate FAC filaments with FAC strengths that fall below a threshold value of 0.1 nA/m^2 (as employed by SWMF) at R_0 in the magnetosphere. Typical maximum values of the current density J are about 1 μA/m^2. We tested our implementation to see whether implementing a similar elimination made any difference in terms of results and computation time. The difference in **ΔB** values that were obtained using the reduced set of FAC filaments compared to the calculation using the full set typically was less than 1% of the signal but could reach up to 5% during quiet times. With our implementation of the calculation in the Interactive Data Language (IDL® by Exelis Vis), we did not notice a significant reduction in terms of the execution time and chose to retain the full set of filaments. The lack of speedup

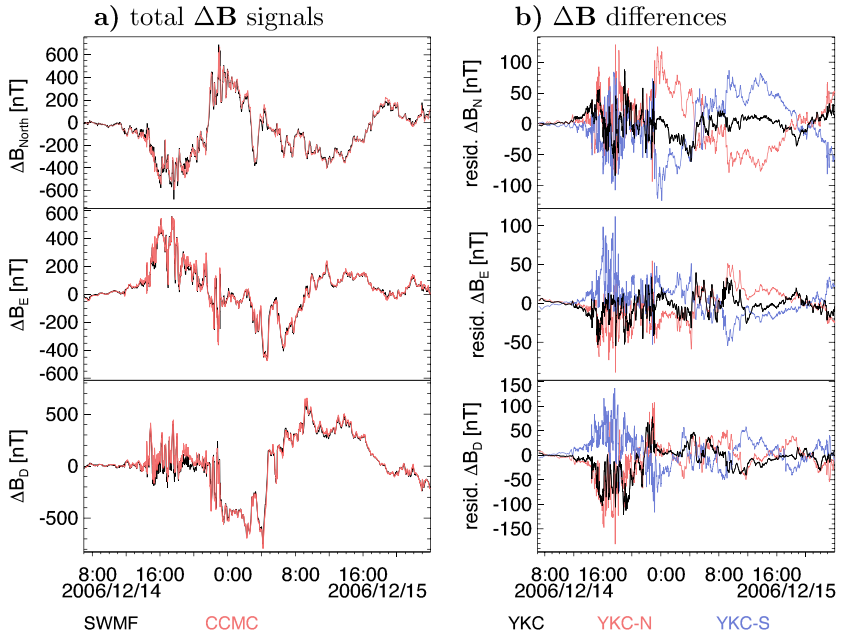

Figure 3. Effect of station location on ionosphere current contribution to Δ**B** at YKC. (a) Ionosphere current contribution: SWMF (black trace), CalcDeltaB using the station locations in geographic coordinates (red). (b) Differences between CalcDeltaB and SWMF at YKC (black) and the effect within CalcDeltaB when the station was moved 1° away (north: "YKC-N" (red), south: "YKC-S" (blue)).

using the elimination procedure may be explained by the fragmentation of large data arrays which are used in the summation. Larger, contiguous data arrays may be processed as fast (or even faster) than several arrays that have a shorter combined length. We chose to keep the full set of FAC filaments to determine the magnetic perturbations and were able to perform the calculation for the 12 stations faster than real time using the radial resolution that is sufficient to provide high-quality results.

6.4. Role of Station Locations in Geomagnetic Coordinates

From the FAC signal we see a difference between our calculated signals and the results from the SWMF model. To assess one possible source of the difference, we use the magnetometer station locations in geographic coordinates (GEO) obtained from the International Real-time Magnetic Observatory Network (INTERMAGNET) website (http://www.intermagnet.org) and the magnetic coordinates (MAG) as specified in a list in Table 2. During the definition of the 2008 challenge, the list was compiled for the 2008 GEM modeling challenge (http://ccmc.gsfc.nasa.gov/GEM_metrics_08) and the positions in magnetic coordinates were specified using International Geomagnetic Reference Field (IGRF) with parameters valid during 2000–2005. These parameters fit the magnetic field conditions for the four original events defined for the GEM challenge, and these positions were used by the SWMF model. Magnetic latitudes and longitudes, however, are time dependent in our postprocessing algorithm. We start with geographic coordinates and convert them to magnetic coordinates for each event using the applicable parameters specified by the IGRF for the year of each event. To perform the coordinate transformation in our postprocessing, we use GEOPACK-2008 with IGRF-11 [*Finlay et al.*, 2010] coefficients that are definitive through year 2010 and constitute extrapolations through year 2015. Figure 3a shows the results of our calculation relative to the SWMF results for the ionosphere, usually the strongest overall signal. Only the result using the geographic station location is shown, the calculation using the geomagnetic location of the station produces nearly identical results. On the global scale shown in Figure 3a, the ionosphere signals agree well. The difference between the two calculations as shown by the black line in Figure 3b for each component of Δ**B** indicates that there can be considerable differences at times within the event that can reach a level of 25% of the total signal (up to 120 nT compared to the global level of ~500 nT).

We note that the SWMF approach to transform coordinates uses a fixed dipole orientation: geographic latitude 79.0°, longitude 289.1°. This does not only affect the transformation between geographic and magnetic coordinates of the station locations (which could be eliminated by using station locations in magnetic

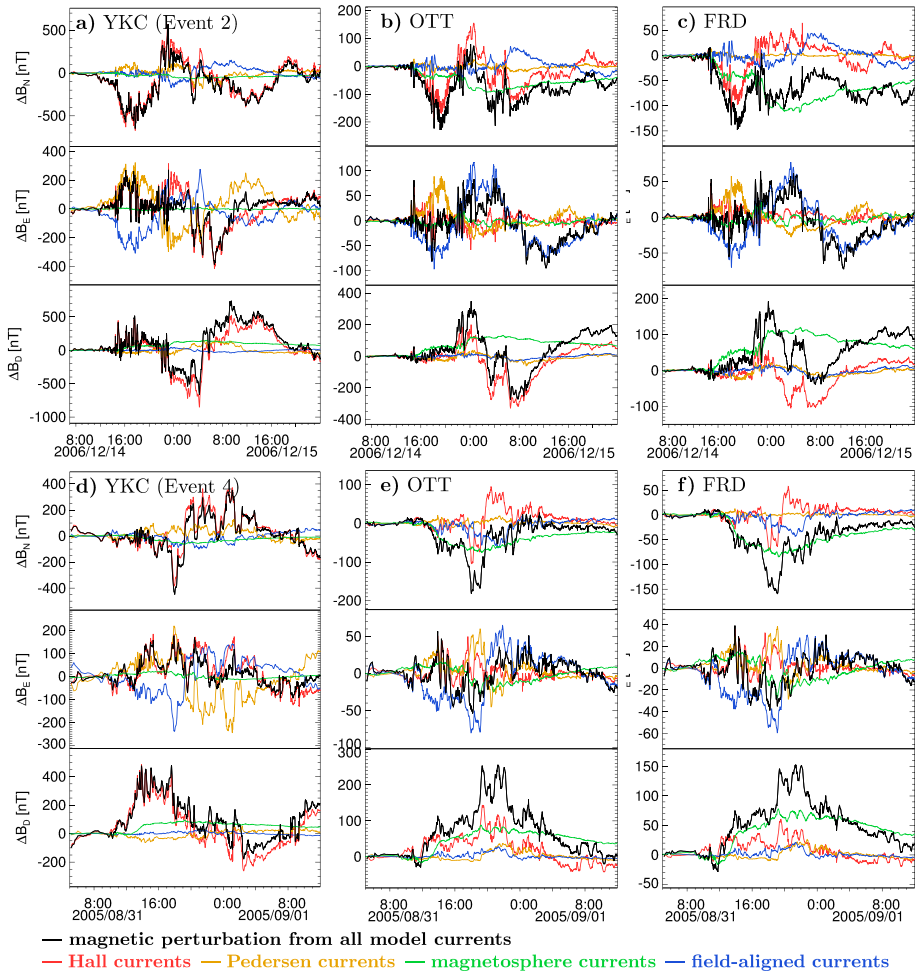

Figure 4. Current system contributions to Δ**B**. (a–c) The components of Δ**B** at the high-latitude station YKC, the midlatitude station OTT, and the low-latitude station FRD for Event 2. (d–f) The perturbations at the same stations for Event 4.

coordinates in our postprocessing tool) but also the transformation between GSM and SM coordinates that affect the contribution from the magnetosphere on the magnetic perturbation. The SWMF coordinate transformation typically results in a station location in Solar Magnetic (SM) coordinates that is of the order of 1° away from the position calculated by GEOPACK 2008 and applicable IGRF coefficients. GEOPACK and IGRF place the geomagnetic pole at a latitude of 79.6° and a longitude of 288.4° for 1 January 2010 and at a latitude of 80.0° and a longitude of 287.8° for 1 January 2010. These positions are at least 1° away from the SWMF specification mentioned before. This fact is demonstrated by plotting the change in Δ**B** obtained within CalcDeltaB for virtual station positions located 1° away north and south of Yellowknife (YKC) as shown by the red and blue traces in Figure 3b in addition to the black line showing the difference between CalcDeltaB and SWMF results at YKC. A 1° displacement of the station does give rise to a change of the Δ**B** signal that is comparable to the observed discrepancy. For Event 2, the SWMF signal at station YKC resembles best the signal obtained for a slight (less than 1°) northern deviation (compare black trace with the red trace) early in the event (on 14 December 2006).

We see that contributions to Δ**B** from ionosphere currents can be strongly affected by a misrepresentation of a station location. Current filaments may be located nearly overhead, and a shifted station location may change the magnitude and even direction of the magnetic contribution from that filament. Contribution from FACs (not shown) also exhibits this effect. The magnetosphere contribution is less affected by a possible error in the station location since the magnetic field perturbation exists on a larger spatial scale, and an error in the station location only slightly changes the spherical (North, East, and Down) components of Δ**B**.

	Event 1			Event 2			Event 3		
Station	North	East	Down	North	East	Down	North	East	Down
FRN	HFMP	FPHM	HMPF	MHFP	FHMF	MHFP	MHFP	FMHP	MHFP
FUR	HFMP	FPHM	HMPF	HMFP	FPHM	HMFP	MHFP	FMHP	MHPF
FRD	HFMP	FPHM	HPMF	MHFP	FPHM	MHFP	MHFP	FPMH	MHPF
WNG	HFPM	FHPM	HMPF	HMFP	FPHM	HMPF	MHFP	FHPM	MHPF
NEW	HFPM	PFHM	HPMF	HFMP	FHPM	HMFP	MHFP	FHPM	HMPF
OTT	HFPM	PFHM	HPMF	HFMP	FHPM	MHPF	MHFP	FPHM	HMPF
MEA	HPMF	HPFM	HPMF	HFMP	FHPM	HMFP	HFMP	FPHM	HMPF
PBQ	HPFM	HPFM	HPMF	HFMP	FPHM	HMPF	HFPM	PFHM	HMPF
ABK	HPFM	HPFM	HPMF	HPFM	HPFM	HPMF	HFPM	FPHM	HMPF
YKC	HPFM	HPFM	HPMF	HPFM	FHPM	HMPF	HFPM	PFHM	HMPF
HRN	HFPM	HPFM	HPMF	HFPM	HFPM	HPMF	HFPM	HPFM	HPMF
IQA	HFPM	HPFM	HPMF	HPFM	HFPM	HPMF	HFPM	HPFM	HPMF
	Event 4			Event 5			Event 6		
Station	North	East	Down	North	East	Down	North	East	Down
FRN	MHFP	FHPM	MHFP	HMFP	HFPM	MHPF	HFMP	HFPM	HFMP
FUR	MHFP	FHPM	MHFP	HMFP	FHPM	MHFP	HFMP	HFPM	HMFP
FRD	MHFP	FHPM	MHFP	HMFP	PHFM	MHFP	HFMP	FPHM	HMFP
WNG	HMFP	FPHM	HMPF	HMFP	HFPM	HMFP	HFMP	HFPM	HMFP
NEW	MHFP	FHPM	MHFP	HMFP	FHPM	HMPF	HFPM	HFPM	HFMP
OTT	MHFP	FHPM	MHFP	HMFP	FHPM	HMFP	HFPM	FPHM	HMFP
MEA	HMFP	PFHM	HMPF	HFMP	FPHM	HMPF	HFPM	HPFM	HFMP
PBQ	HPFM	HFPM	HPMF	HFPM	PFHM	HMPF	HFPM	HPFM	HPFM
ABK	HPFM	HPFM	HMPF	HFPM	HPFM	HMPF	HFPM	HFPM	HFPM
YKC	HPFM	HPFM	HMPF	HPFM	FPHM	HMPF	HPFM	HPFM	HFPM
HRN	HPFM	HFPM	HMPF	HFPM	HFPM	HMPF	HPFM	HFPM	HFMP
IQA	HPFM	HFPM	HPMF	HPFM	PFHM	HMPF	HPFM	HPFM	HFMP

Figure 5. Relative importance of current systems. H: Hall, P: Pedersen, F: field-aligned currents., and M: magnetosphere. Contributions with strongest root-mean-square magnitudes are listed first, followed by successively weaker contributions. Stations are grouped in four categories: low latitudes (three stations, not used in d*B*/d*t* metrics study), midlatitudes (three of four stations used in study, bold), auroral zone ("high latitude," three stations used in study, bold), and polar region (two stations, not used in study). The colors of the letters correspond to the colors of the traces in Figure 4 at the example stations.

7. Results: Relative Importance of Current Contributions

Using the new postprocessing tool CalcDeltaB, we can investigate the relative contributions of the various current systems to the magnetic perturbations on the ground. Figure 4 shows a sample of relative strength of the contributions of current systems to the overall $\Delta\mathbf{B}$ signal. We plotted the contributions for one low-latitude station (FUR), one midlatitude station (OTT), and one auroral-latitude station (YKC) for Event 2 (Figures 4a–4c) and Event 4 (Figures 4d–4f). The ionosphere contribution is divided into Hall current (red) and Pedersen current (yellow) contributions in the ionosphere, FACs (blue), and magnetosphere (green). The total calculated signal is shown in black.

Typically, the Hall contributions dominate for North and Down components (top and bottom set of traces in Figures 4a–4f). The stations located farthest north (Figures 4a and 4d) show closest agreement between the Hall current contribution and the overall northward $\Delta\mathbf{B}$ signal. The lower the latitude the higher the influence from magnetosphere currents: stations in the midlatitudes (Figures 4b and 4e) and stations closest to the equator (Figures 4c and 4f) show a large (often dominant) influence from the magnetosphere current contribution (green).

The eastern component of $\Delta\mathbf{B}$ (set of traces in the middle of Figures 4a–4f) is often dominated by the FAC contribution (shown in blue), especially for lower latitudes (Figures 4b–4f). In some instances, the FAC and Pedersen current contributions (blue and yellow) may be of comparable strength compared to the Hall contribution but may partially cancel each other (Figures 4a and 4d for the east component at high latitudes). This has been known and justifies using only Hall currents at auroral latitudes since effects that form magnetosphere currents are small to negligible. The cancelation between contributions from FACs and Pedersen currents is seen at times in midlatitude stations as well (Figures 4b and 4e).

In Figure 5 the contributions ("H" for Hall, "P" for Pedersen, "F" for FAC, "M" for magnetosphere) are ranked by using the standard deviation from each contribution's averages as a measure of strength for all stations and all six events. The distribution shown confirms the observations described above for all events:

1. Current systems exhibit a different influence on the east component than on the north and down components.
2. Hall component dominates North and Down components, especially for high latitudes, followed by Pedersen currents, FACs, and magnetosphere (with few exceptions).
3. FAC contributions dominate the East component for midlatitudes and low latitudes and are comparable to Hall and Pedersen current contributions for high latitudes. Even though Hall currents may yield a stronger contribution, they are partially canceled by Pedersen currents, making the FAC component dominate the final signal.

4. Magnetospheric currents dominate the magnitude of low-latitude magnetic perturbations but play a small role in high latitudes. Generally, magnetosphere currents provide a varying baseline (changing on the scale of hours) rather than a short-term signal (changing within minutes). The short-term signal is provided by Hall currents more than the magnetosphere in all cases (see Figures 4a, 4b, 4d, and 4e).

These findings are consistent with results presented in Figures 1–3 of *Yu et al.* [2010] for the 4 May 1998 event. We find that the relative strength of the four current systems is not always the same for a given station between events, and we see contribution of comparable strength switch places in the rankings shown in Figure 5. A complete set of time series plots similar to Figure 4 may be viewed in the supporting information submitted with this paper.

8. Discussion

Magnetic field perturbations on the ground drive geomagnetic induction phenomena that can lead to hazardous electric currents in long technological conductor systems such as electric power lines. It is thus of major interest to better specify and predict the field perturbations or dB/dt. The calculation of magnetic perturbations on the ground from first-principle models of the magnetosphere and ionosphere adds valuable information to the outputs of first-principle magnetosphere-ionosphere simulation models that can be directly compared to observational data obtained on the ground. Model predictions thus can be validated against ample ground-based data in addition to using sparser space-based observations.

We have implemented an efficient suite to calculate magnetic perturbations on the ground from all the electric current systems in the coupled ionosphere-magnetosphere. Using SWMF model outputs we validated our calculations against the implementation of the same calculation in SWMF described by *Yu et al.* [2010]. The dB/dt study [*Pulkkinen et al.*, 2013] validated the use of CalcDeltaB by demonstrating significant skill to specify time derivatives of $\Delta\mathbf{B}$ against selected threshold values. The stand-alone calculation method can be applied to outputs from all the major global magnetohydrodynamic magnetosphere models and was used in the dB/dt study for the SWMF, OpenGGCM, and LFM models. It is easy to extend this method to any additional model of the magnetosphere-ionosphere system that will be supported at the CCMC (e.g., GUMICS). To make this tool available to users in the scientific community, we plan to integrate the calculations into the Kameleon access and interpolation library (available for download from the CCMC web site) as we complete the support of ionosphere electrodynamics outputs from all models in addition to the magnetosphere outputs in Kameleon.

The placement of positions around a given magnetometer position allows us to estimate the variability of the magnetic perturbation predicted by a model based on location changes on the ground (or the shift of ionospheric currents in the model compared to observations). Further studies will be conducted to develop suitable ensemble modeling to find a likely range of model predictions for any location which is essential for space weather research and applications.

In the computations described here, we do not include contributions to $\Delta\mathbf{B}$ that arise from the presence of the Earth and the resulting shielding and geomagnetic induction effects. The proper treatment of these effects requires the knowledge of local conditions (i.e., the spatial distribution of conductivities below the surface) at each magnetometer station and the use of the time history of electric currents rather than snapshots of currents used here and in the dB/dt study. Results obtained with CalcDeltaB and within SWMF are far from perfect but have been shown in the dB/dt study to have significant correlation with the observations and to produce statistically useful predictions of dB/dt exceeding certain thresholds (with Heidke Skill Scores surpassing 0.7 where 1 is a perfect score and above-zero values denote skills better than random predictions). In the absence of a full electromagnetic propagation model, the magnetic perturbation $\Delta\mathbf{B}$ as calculated by the SWMF model or with this new tool can be used to predict the time derivative dB/dt that is relevant for space weather forecasting either with time differencing or using an empirical relationship [*Tóth et al.*, 2014].

In addition to not accounting for geomagnetic induction effects in the calculation of magnetic perturbations, the underlying modeling of the magnetosphere-ionosphere system certainly needs improvement as well: We need more realistic ionosphere conductances and multifluid, hybrid, or kinetic modeling of the magnetosphere to better specify precipitation patterns and currents into the ionosphere that determine conductances and ionospheric currents. Ideally, the current system between the magnetosphere and

the ionosphere would be modeled without resorting to a gap region between the two, now filled with field-aligned currents only. In the future, improvements in coupled global magnetosphere-ionosphere models (and thus results from CalcDeltaB) will be recognized as new model versions will be subject to challenges similar to the 2008 GEM Modeling Challenge or the recent d*B*/d*t* challenge.

Acknowledgments
Solar wind input data for the models (magnetic field and plasma parameters) were obtained from CDAweb (http://cdaweb.gsfc.nasa.gov). The authors thank A. Glocer (NASA GSFC) for valuable feedback and discussion while interpreting discrepancies between our results with $\Delta\mathbf{B}$ computed by the SWMF model. Magnetometer observations were obtained via INTERMAGNET (http://www.intermagnet.org/). We used Eric Dennison's online calculator of the magnetic field caused by a current loop (http://www.netdenizen.com/emagnet/offaxis/iloopcalculator.htm) to check our analytic results and thank him for the reference for equation (12).

References

Abramowitz, M. (2010), *Handbook of Mathematical Functions with Formulas, Graphs, and Mathematical Tables*, United States National Institute of Standards and Technology, Gaithersburg, Maryland.

DeZeeuw, D. L., S. Sazykin, R. A. Wolf, T. I. Gombosi, A. J. Ridley, and G. Tóth (2004), Coupling of a MHD code and an inner magnetospheric model: Initial results, *J. Geophys. Res.*, *109*, A12219, doi:10.1029/2003JA010366.

Finlay, C. C., et al. (2010), International geomagnetic reference field: The eleventh generation, *Geophys. J. Int.*, *183*, 1216–1230, doi:10.1111/j.1365-246X.2010.04804.x.

Griffiths, D. J. (1950), *Introduction to Electrodynamics*, Mc Graw-Hill, New York.

Lyon, J. G., J. A. Fedder, and C. M. Mobarry (2004), The Lyon-Fedder-Mobarry (LFM) global MHD magnetospheric simulation code, *J. Atmos. Sol. Terr. Phys.*, *66*, 1333–1350, doi:10.1016/j.jastp.2004.03.020.

Merkin, V. G., and J. G. Lyon (2010), Effects of the low-latitude ionospheric boundary condition on the global magnetosphere, *J. Geophys. Res.*, *115*, A10202, doi:10.1029/2010JA015461.

Powell, K. G., P. L. Roe, T. J. Linde, T. I. Gombosi, and D. L. De Zeeuw (1999), A solution-adaptive upwind scheme for ideal magnetohydrodynamics, *J. Comput. Phys.*, *154*(2), 284–309, doi:10.1006/jcph.1999.6299.

Pulkkinen, A., et al. (2011), Geospace environment modeling 2008-2009 challenge: Ground magnetic field perturbations, *Space Weather*, *9*, S02004, doi:10.1029/2010SW000600.

Pulkkinen, A., et al. (2013), Community-wide validation of ground magnetic field perturbation predictions of Geospace models to support model transition to operations, *Space Weather*, *11*, 369–385, doi:10.1002/2013SW000990.

Raeder, J., et al. (2001), Global simulation of the Geospace environment modeling substorm challenge event, *J. Geophys. Res.*, *106*(A1), 381–395, doi:10.1029/2000JA000605.

Rastätter, L., et al. (2013), Geospace environment modeling 2008-2009 challenge: *Dst* index, *Space Weather*, *11*, 187–205, doi:10.1002/swe.20036.

Ridley, A. J., T. I. Gombosi, and D. L. De Zeeuw (2004), Ionospheric control of the magnetospheric configuration: Conductance, *Ann. Geophys.*, *22*, 567–584.

Tóth, G., et al. (2005), Space weather modeling framework: A new tool for the space science community, *J. Geophys. Res.*, *110*, A12226, doi:10.1029/2005JA011126.

Tóth, G., et al. (2012), Adaptive numerical algorithms in space weather modeling, *J. Comput. Phys.*, *231*(3), 870–903, doi:10.1016/j.jcp.2011.02.006.

Tóth, G., X. Meng, T. I. Gombosi, and L. Rastätter (2014), Predicting the time derivative of local magnetic perturbations, *J. Geophys. Res. Space Physics*, *119*, 310–321, doi:10.1002/2013JA019456.

Wiltberger, M., W. Wang, A. G. Burns, S. C. Solomon, J. G. Lyon, and C. C. Goodrich (2004), Initial results from the coupled magnetosphere ionosphere thermosphere model: Magnetospheric and ionospheric responses, *J. Atmos. Sol. Terr. Phys.*, *66*, 1411–1423, doi:10.1016/j.jastp.2004.03.026.

Wolf, R. A., R. W. Spiro, and F. J. Rich (1991), Extension of convection modeling into the high-latitude ionosphere—Some theoretical difficulties, *J. Atmos. Terr. Phys.*, *53*, 817–829, doi:10.1016/0021-9169(91)90096-P.

Yu, Y., A. Ridley, D. T. Welling, and G. Tóth (2010), Including gap region field-aligned currents and magnetospheric currents in the MHD calculation of ground-based magnetic field perturbations, *J. Geophys. Res.*, *115*, A08207, doi:10.1029/2009JA014869.